Waveform tomography in the Mediterranean and southeast Asia

Nienke Blom[1], Andreas Fichtner[2], Alexey Gokhberg[2], Nicholas Rawlinson[1], Deborah Wehner[1]

1: University of Cambridge
2: ETH Zürich

TL;DR [1/2]

Mediterranean:

- (adjoint) waveform tomography inverting for v_{SH}, v_{SV}, v_P and density
- Complex slab structures imaged down to the transition zone
- Strong heterogeneities of O{10%}
- Published in Solid Earth: [Blom et al, Solid Earth, 2020]()

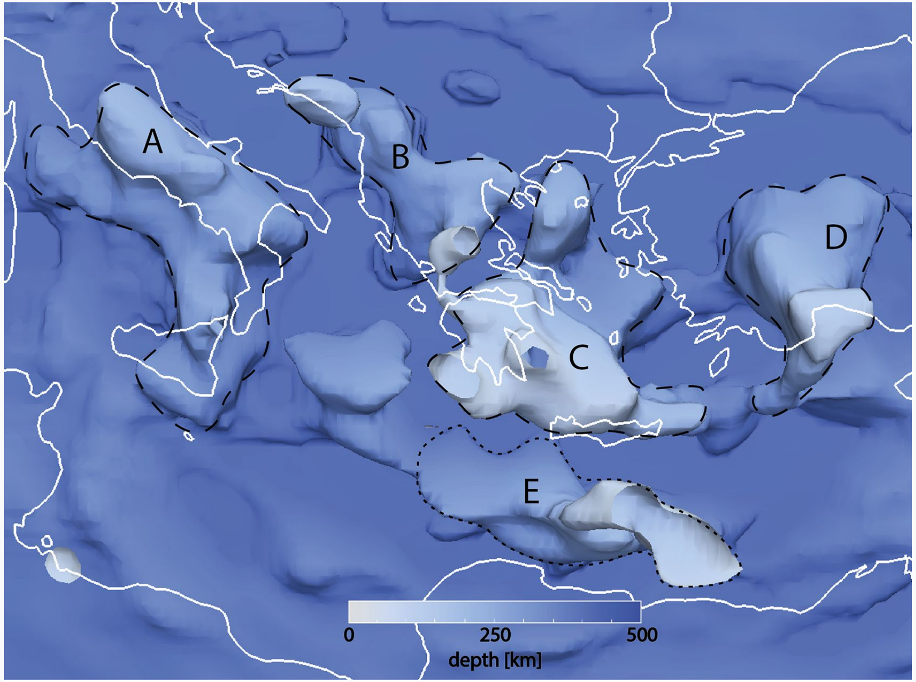

Figure: top view of a 3-D rendering of the final model, coloured by depth. All major subduction zones are clearly visible

TL;DR [2/2]

Southeast Asia:

- New temporary arrays fill gaps in coverage
- Preliminary results show large-scale structures corresponding to known structures.
- More details later this session in the presentation by Deborah Wehner.

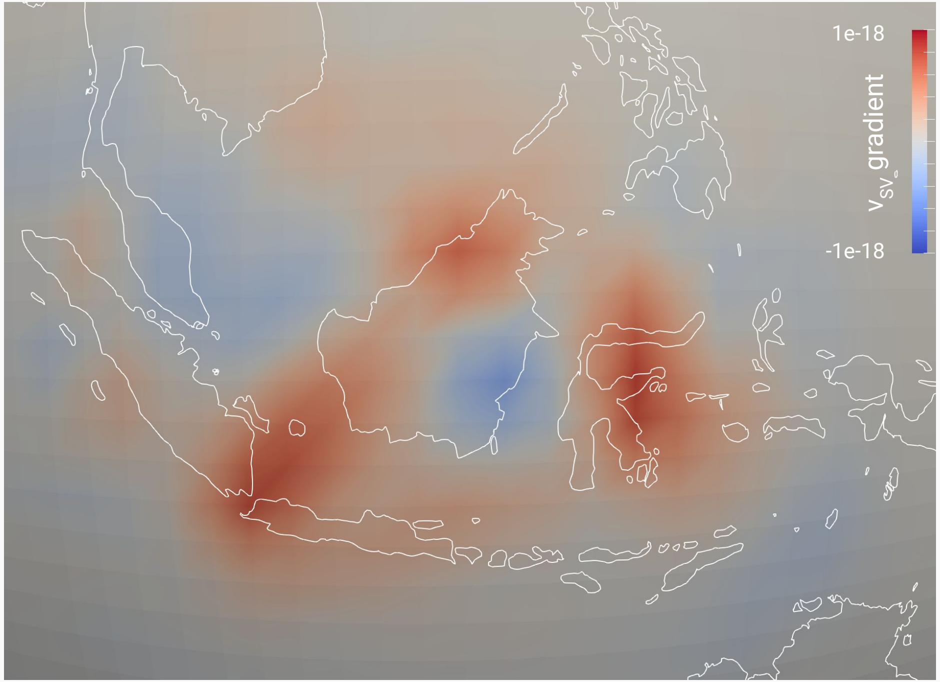

Figure: horizontal slice through the v_{SV} gradient for the initial model based on 18 events.

Contents (click on a section to go there)

Click any

Waveform tomography in the central and eastern Mediterranean

(Blom et al, Solid Earth, 2020)

Tectonic setting

The Mediterranean:

- a complex convergence zone
- dominated by convergence between Africa and Eurasia *(~6 mm/yr [Reilinger et al, 2006])*
- Large plates and plate fragments moving in an anticlockwise fashion

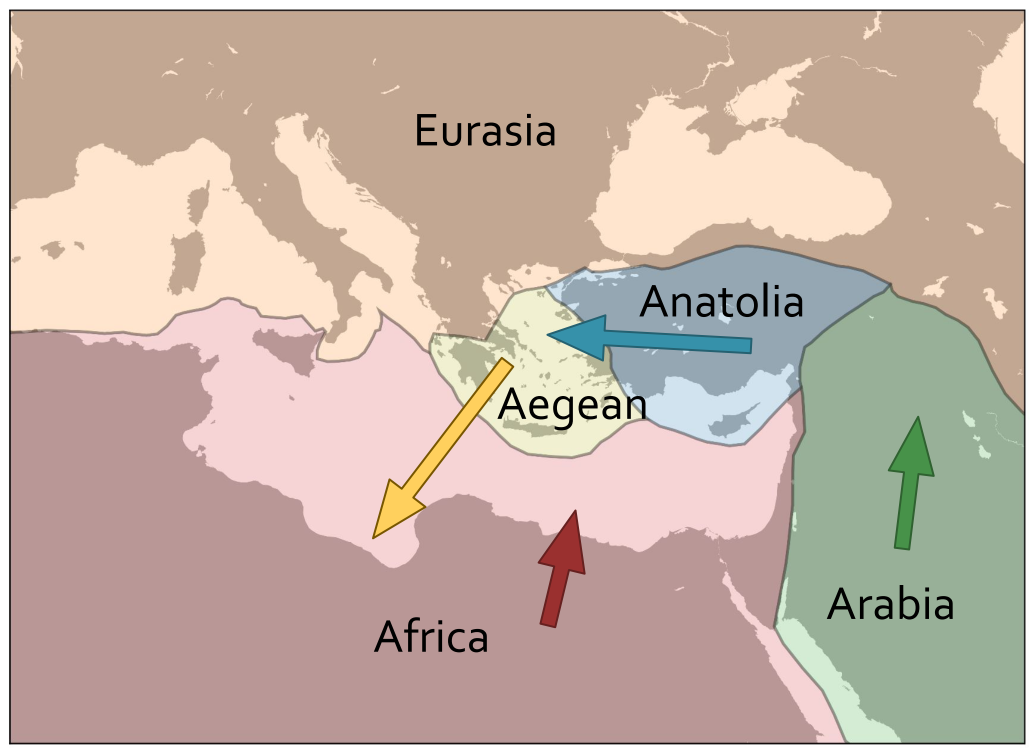

Cartoon after [Blom et al, Solid Earth, 2020](). All motions are shown as relative to Eurasia.

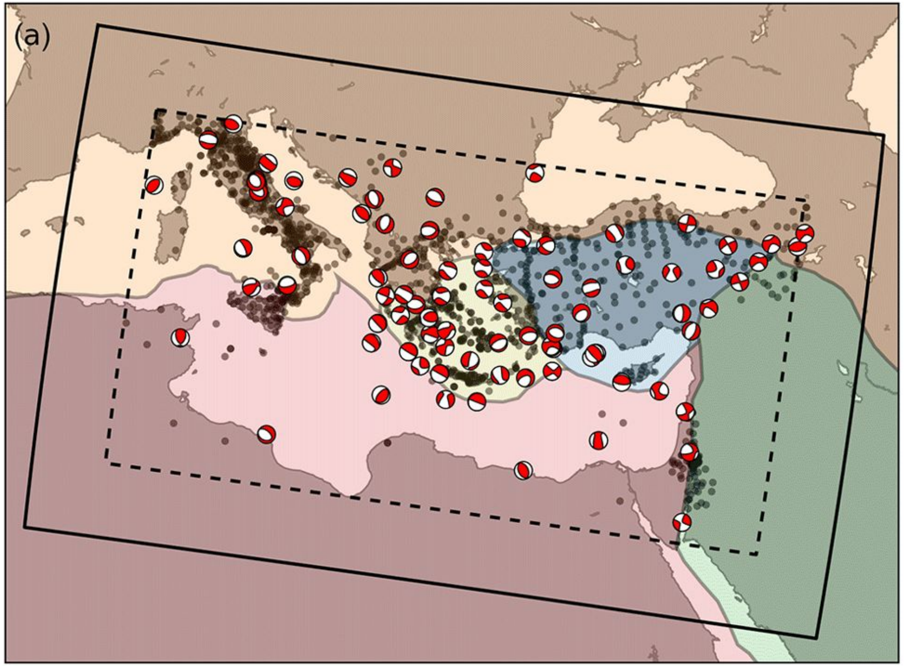

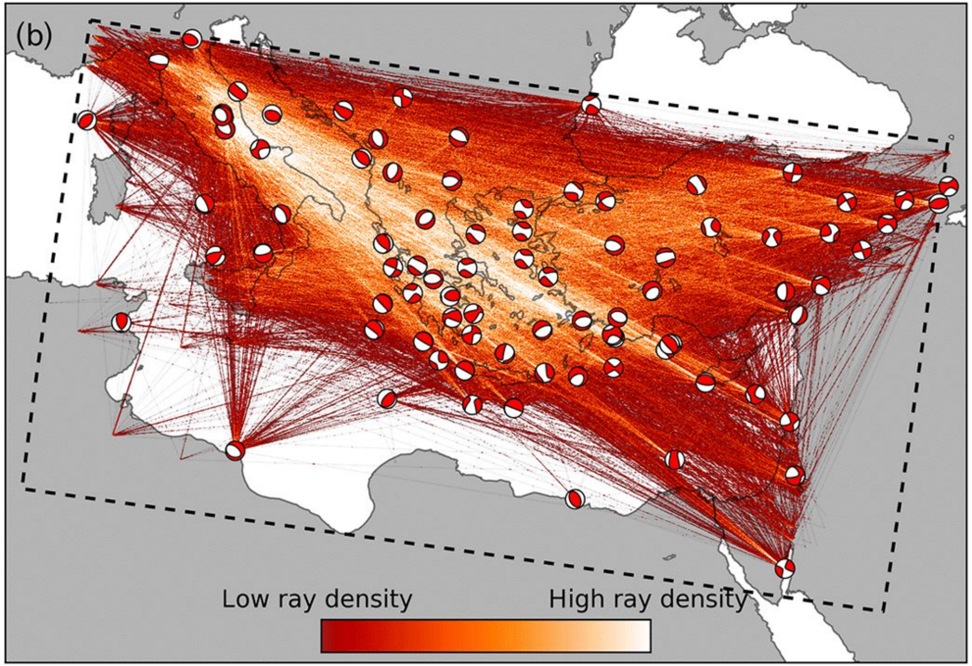

Modelling domain and data: **(a)** The modelling domain in the central and eastern Mediterranean, with tectonic plates taken from Bird (2003): Africa in red, Eurasia in orange, the Aegean plate in yellow, Anatolia in blue and the Arabian plate in green. Superimposed on top of this are the earthquakes used in this study (red–white focal mechanisms) and the locations of all seismic stations (black dots). A 3◦ buffer zone separates the outer and inner model boundaries (solid and dashed lines, respectively). Within the buffer zone, wave propagation energy is absorbed that would otherwise result in artificial reflections. **(b)** An impression of "ray density" in the model domain, based on the great circle paths of all traces used in this study. This is just a rough proxy of coverage, serving only to highlight the variability and directionality of the coverage. (Blom et al, Solid Earth, 2020)

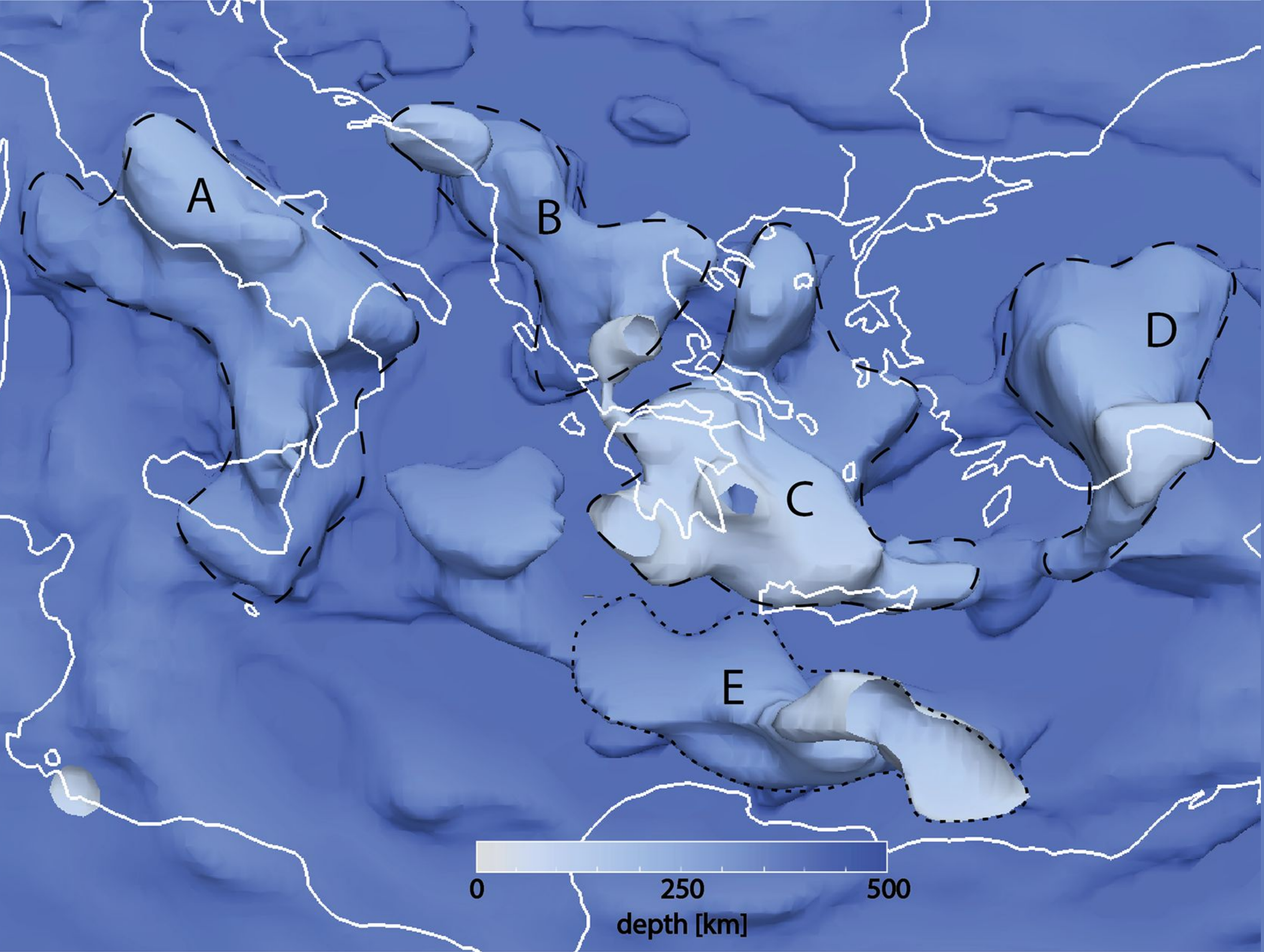

Final model: Top view of a 3-D rendering of high-velocity structures within the model domain. For this figure, the 4.75 km/s isosurface of isotropic S velocity v_S was selected. This value is somewhat above the upper-mantle average and was chosen in order to emphasise the approximate outline of the high-velocity features. Shallower regions are coloured whiter and deeper regions bluer. The high-velocity anomalies are labelled with letters: **A**: Italy / Apennines; **B**: Dinarides, **C**: Hellenic subduction zone, **D**: Anatolia. **E** is possibly an artefact (see bonus material). For a video fly-through see the link in Blom et al, Solid Earth, 2020.

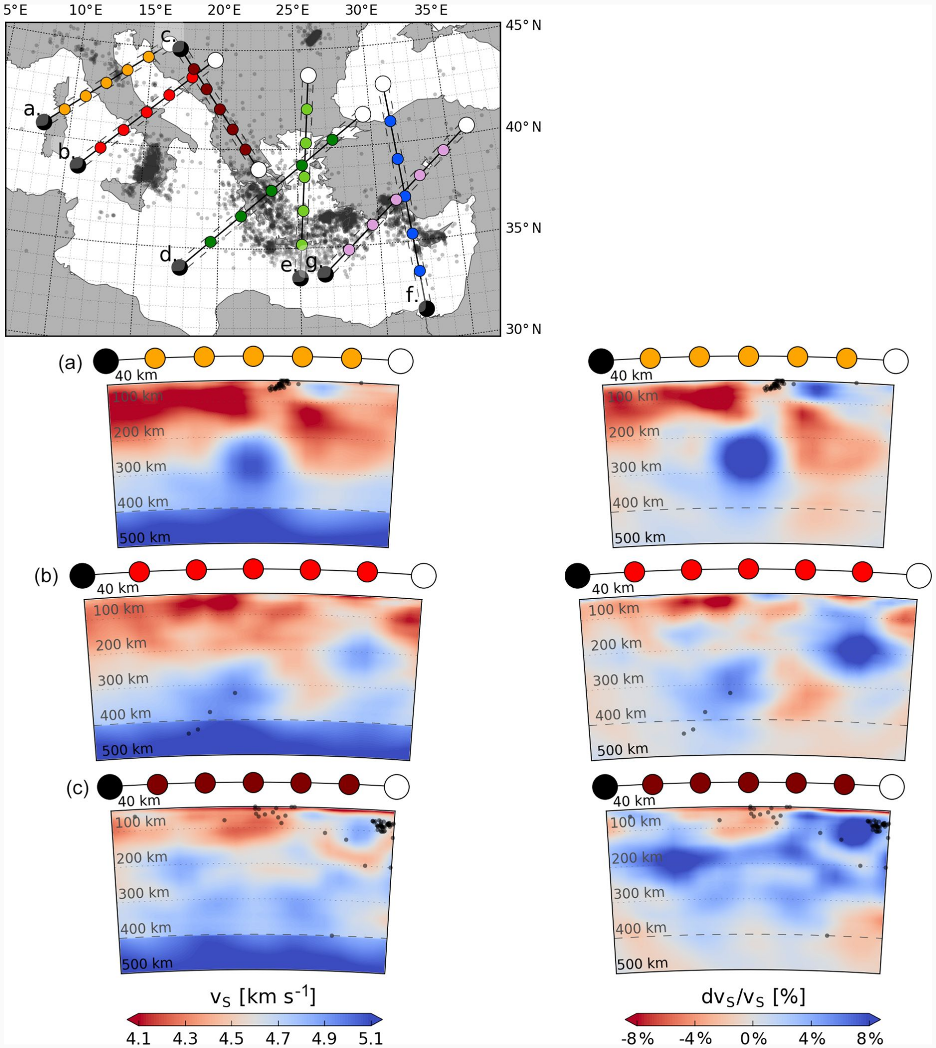

Cross sections through the final model: Cross-sections through the S-velocity model and a map showing their locations. Left column: isotropic S velocity v_S; right column: relative deviations in v_S from the depth-averaged starting model. Black dots indicate seismicity in the region, as obtained from the European–Mediterranean Seismological Centre (EMSC-CSEM) catalogue (2004–August 2019, depths greater than 40 km and M>2; Godey et al., 2013). Seismicity on the cross sections is plotted if it is within 50 km from the cross-section slice. Top: map showing the locations of the cross sections.

(a) Cross section across northern Italy (anomaly A in the previous figure). **(b)** Cross section across Italy and the Dinarides (anomalies A and B). **(c)** Cross section parallel to the Dinaric anomaly (anomaly B).

(continued on next slide)

[(Blom et al, Solid Earth, 2020)]

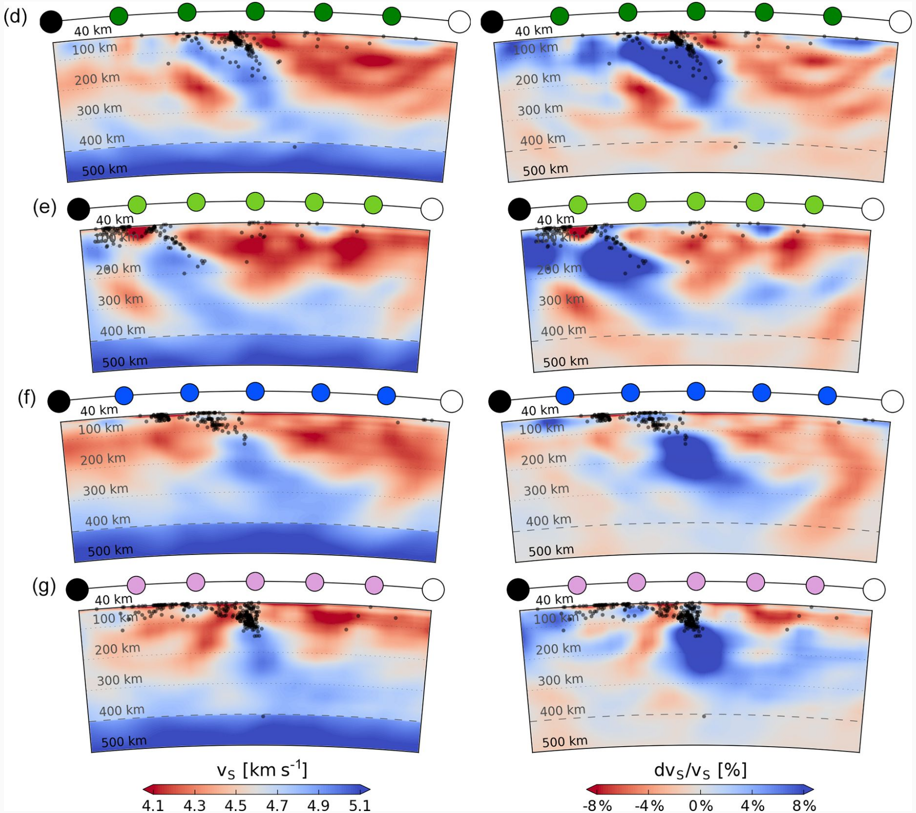

(continuation from previous slide)

(d) Cross section across the Hellenic subduction zone (anomaly C). **(e)** Alternate orientation cross section of the Hellenic subduction zone (anomaly C). **(f)** Cross section across the Anatolian subduction zone (anomaly D). **(g)** Alternate cross section across the Anatolian subduction zone.

[(Blom et al, Solid Earth, 2020)]

Misfit comparison [1/2]: A comparison of the initial and final models in the shortest period band (28–150 s). Misfit is computed with the objective functional:

$$J_{\mathrm{TF},p}(\boldsymbol{m}) := \int_t \int_\omega W_p^2\left(t,\omega\right)\left[\phi(\boldsymbol{m},t,\omega) - \phi_{\mathrm{obs}}(t,\omega)\right]^2 \mathrm{d}t\mathrm{d}\omega,$$

$$W_p = \frac{\log(1+|\tilde{u}_{\mathrm{obs}}|)}{\max(\log(1+|\tilde{u}_{\mathrm{obs}}|))},$$

where ϕ-ϕ_{obs} is the phase shift, and $\tilde{u}$ is the time-frequency representation of seismic signal *u* as calculated via the Gabor transform.

(a) Absolute change in misfit for each of the events. **(b)** Comparison of maximum time-frequency phase shift between observed and synthetic seismograms within windows, for the initial and final models. **(c)** Misfit for the initial and final models, plotted both for the whole dataset (thick bar) and per event (narrow bars). Total misfit decrease in this period band is 48 %. (Blom et al, Solid Earth, 2020)

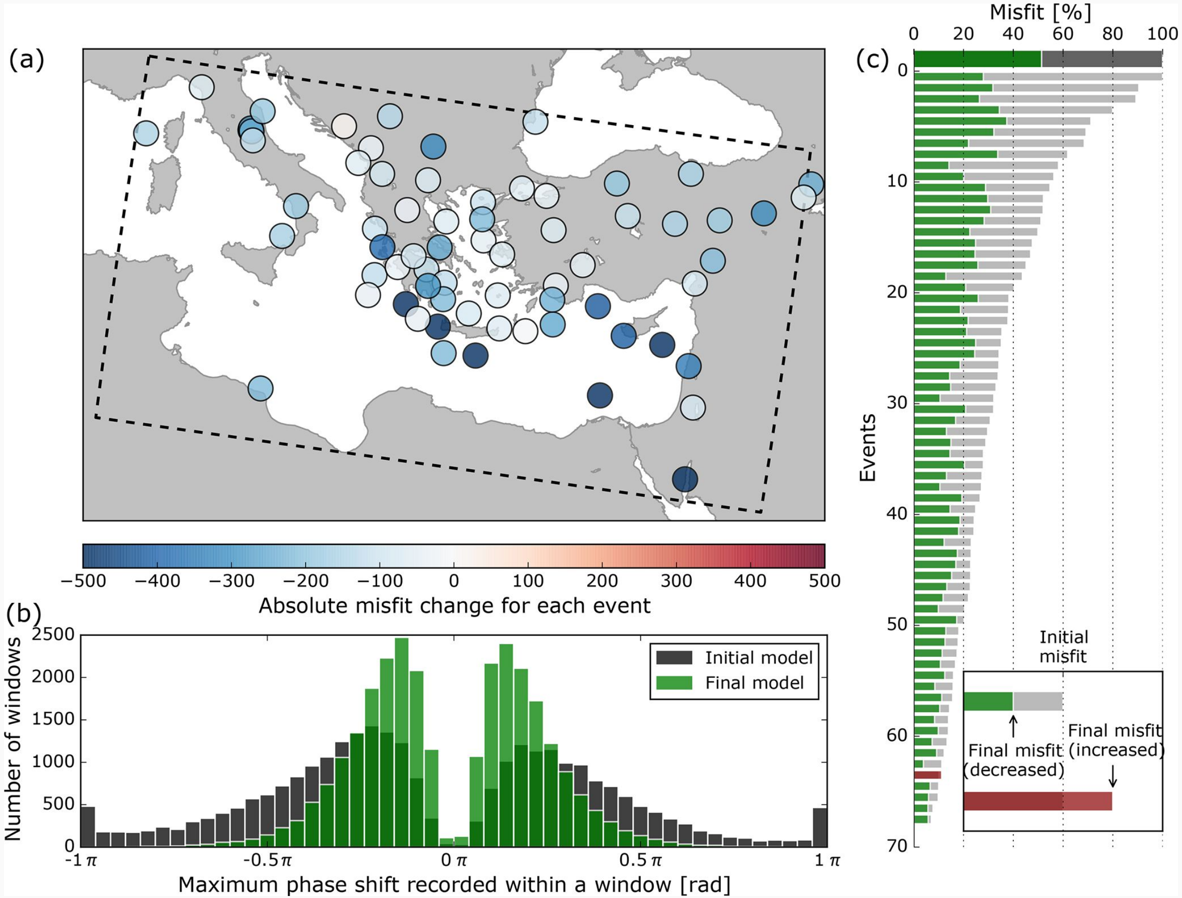

Note: the histograms in panel (b) contain a gap around zero phase shift as a result of the decision algorithm used to select or discard windows, which includes a criterion based on a division by the maximum absolute phase shift within a window. As a result, however, the windows with a near-zero phase shift disappear from the distribution which consequently is very much non-Gaussian. (for full details see the paper)

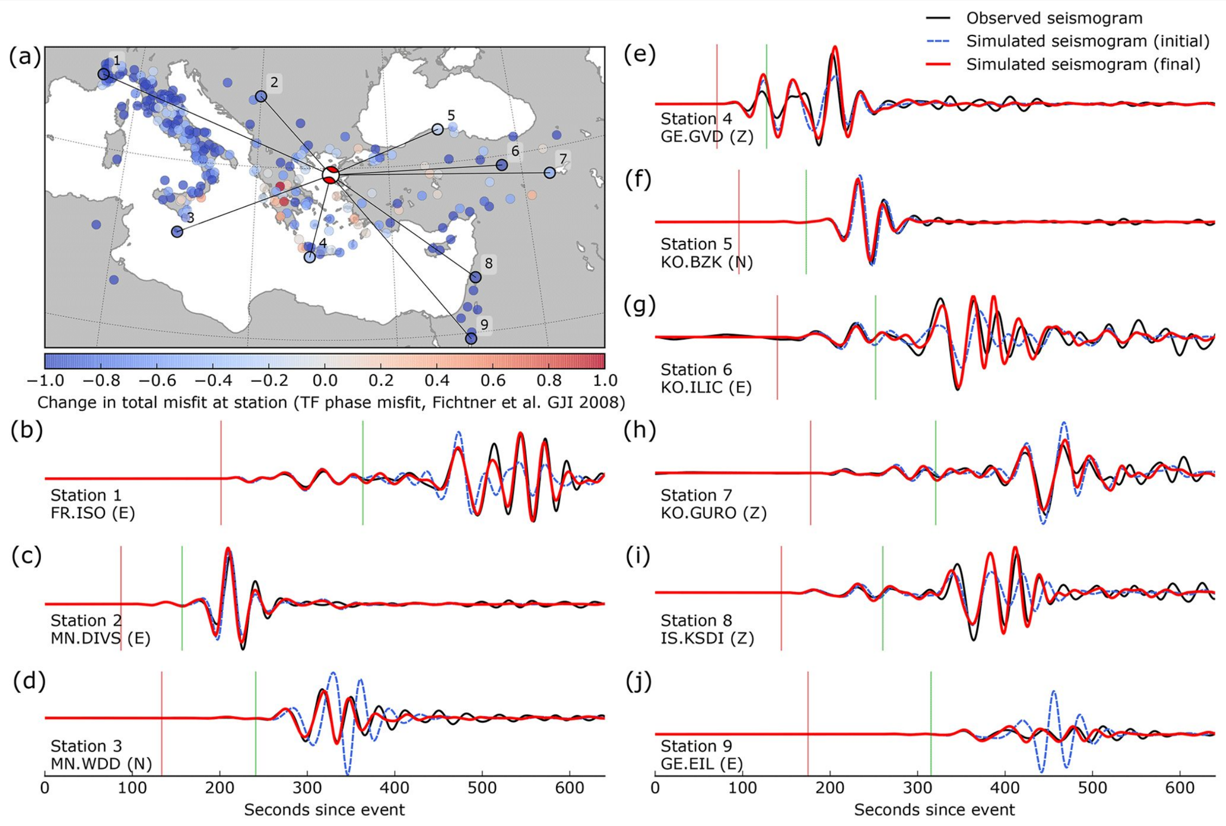

Misfit comparison [2/2]: Misfit change for a single event and example seismograms in the frequency band of 28-150 s. **(a)** Change in misfit for all stations of an event in the Aegean Sea (8 January 2013, 14:16:11 UTC, Mw=5.8), evaluated in period band 7 (28–150 s) (Table 1). Each dot represents the total change in misfit for a station. **(b–j)** Examples comparing observed (black) and synthetic seismograms for the indicated stations (initial model: dashed, pink; final model: red). Vertical lines indicate P-wave (red) and S-wave (green) arrival times predicted for PREM (Dziewoński and Anderson, 1981) using the TauP toolkit (Crotwell et al., 1999) in ObsPy (Beyreuther et al., 2010). [(Blom et al, Solid Earth, 2020)]

For more comparisons for events not used in the inversion, please see the paper

Waveform tomography in southeast Asia

(more details later this session)

Tectonic setting

Southeast Asia:

- An even more complex area with multiple subduction zones
- Displays the strongest seismicity in the world

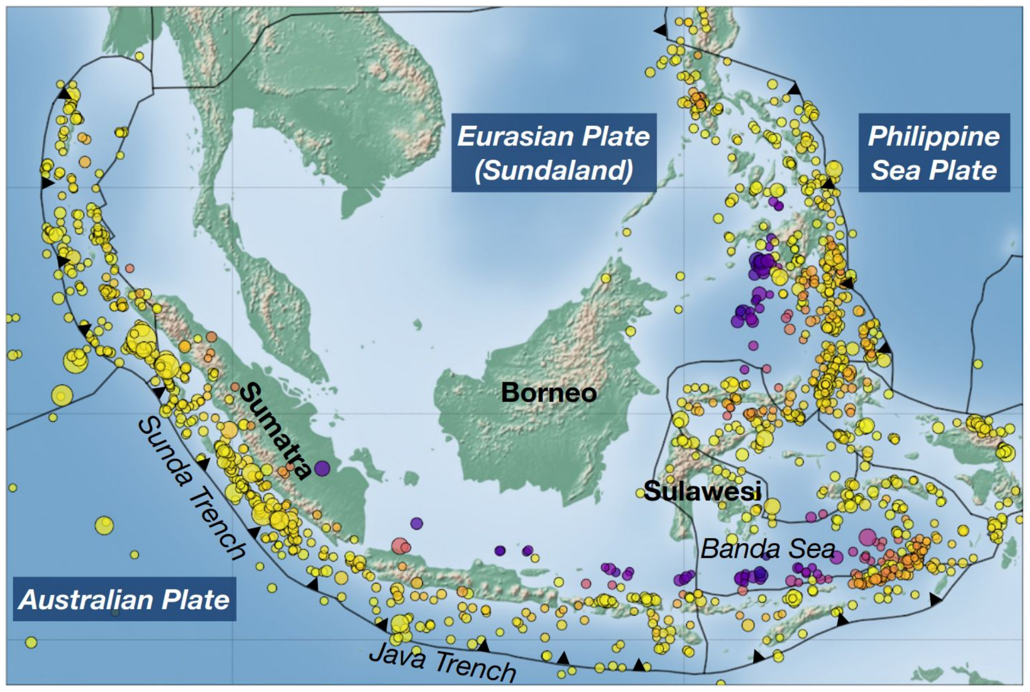

Image: Deborah Wehner

Seismic data

Recently deployed **temporary seismic networks** give an unprecedented coverage of this tectonically complex area, allowing us to use waveform tomography for the first time.

(see also presentations this session by [Deborah Wehner](), [Omry Volk](), [Harry Linang]() and [Simone Pilia]() — [Conor Bacon]() also used this dataset but presented on Monday)

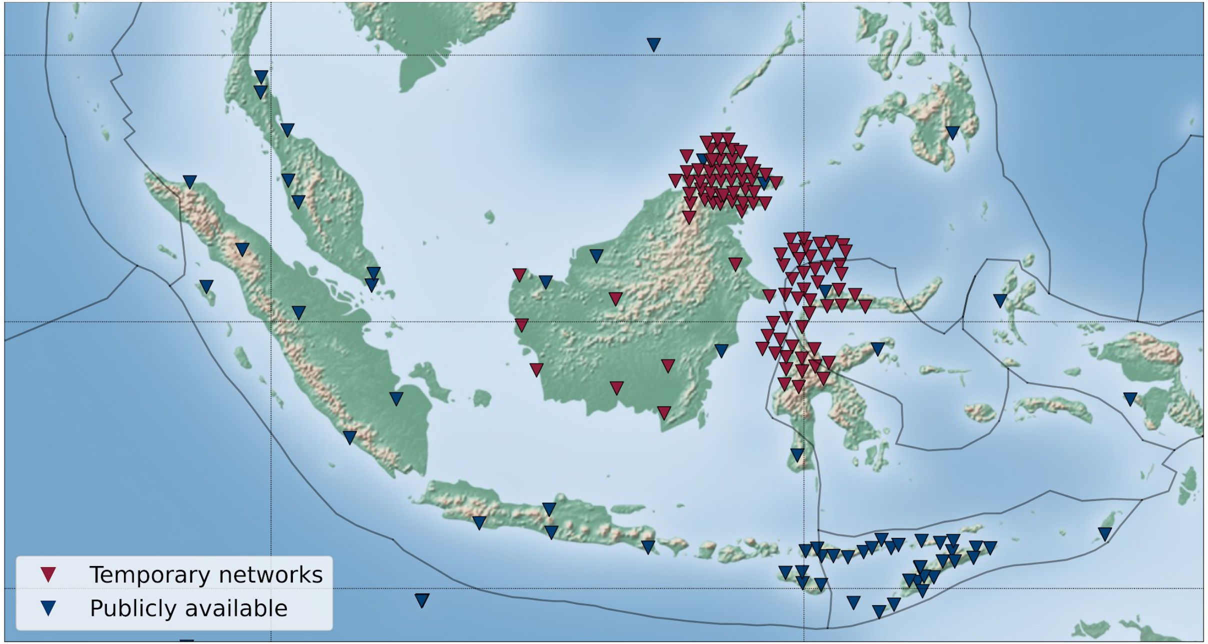

Waveform tomography

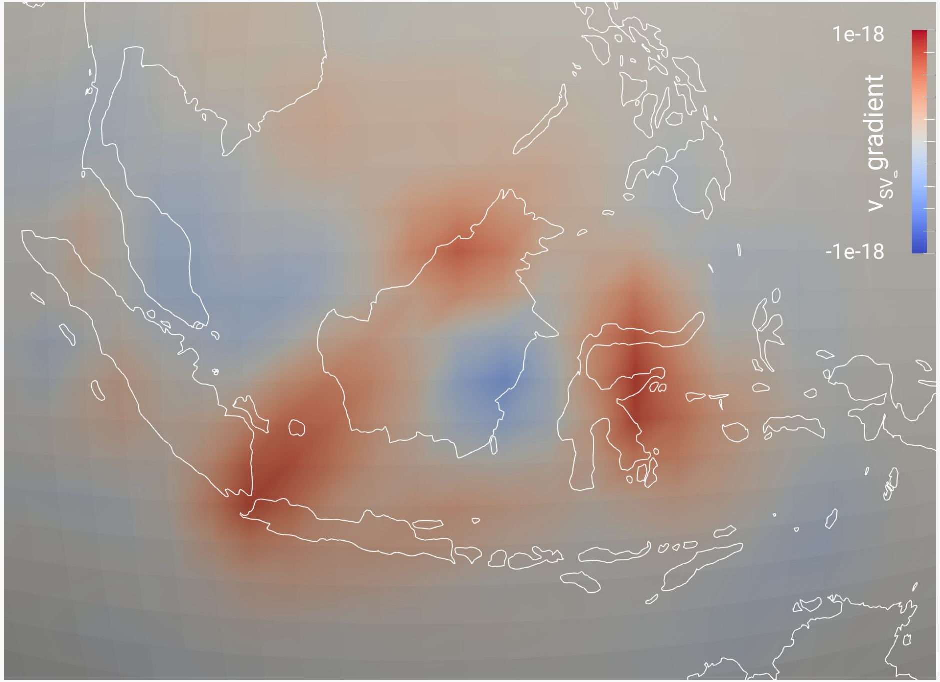

- We use **waveform tomography** with gradient-based iterative inversion and the adjoint method to compute gradients.
- **Preliminary gradients** based on the data from 18 events and filtered at long periods (100-150 s) show large-scale features that show similarities to known geology (e.g. [Zenonos et al, 2019](#)).

Full results presented by [Deborah Wehner](#).

Bonus 1:
Wait, what was (adjoint) waveform tomography again?

Waveform tomography

Waveform tomography compares observed seismograms directly with synthetically computed seismograms. These synthetics are computed using a 3-D solver (**forward modelling**). This makes it computationally expensive.

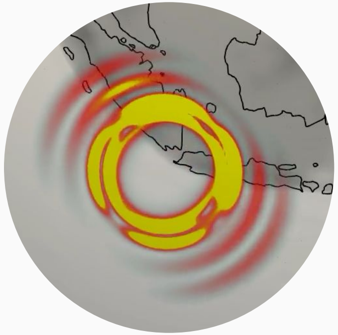

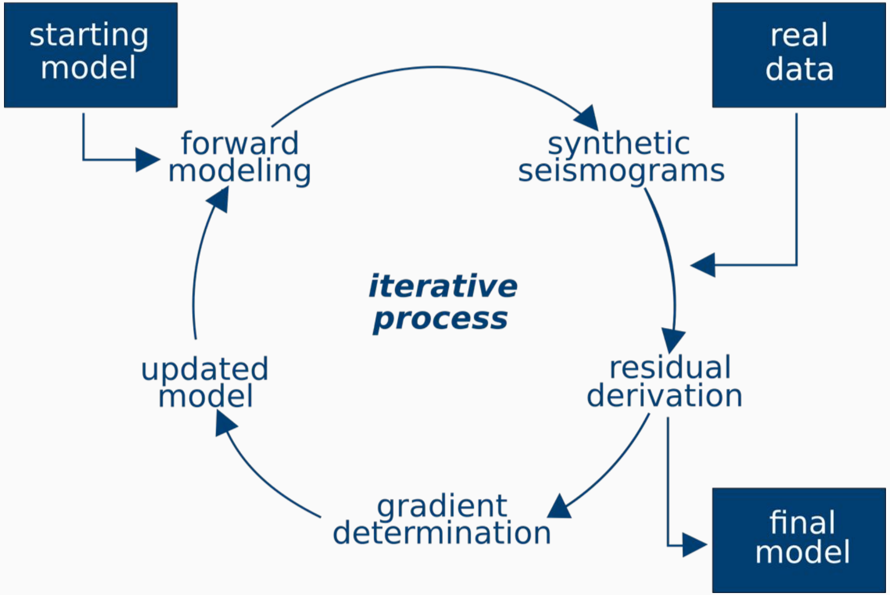

Cartoon by Deborah Wehner

Waveform tomography

The difference between observed and synthetic seismograms is summarised in the **misfit** or **objective functional**.

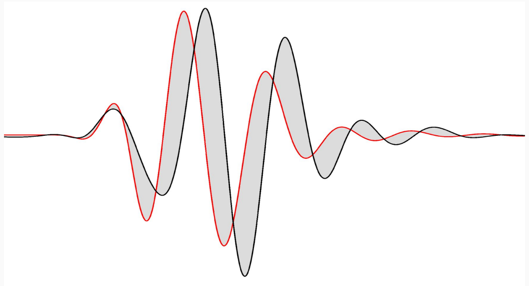

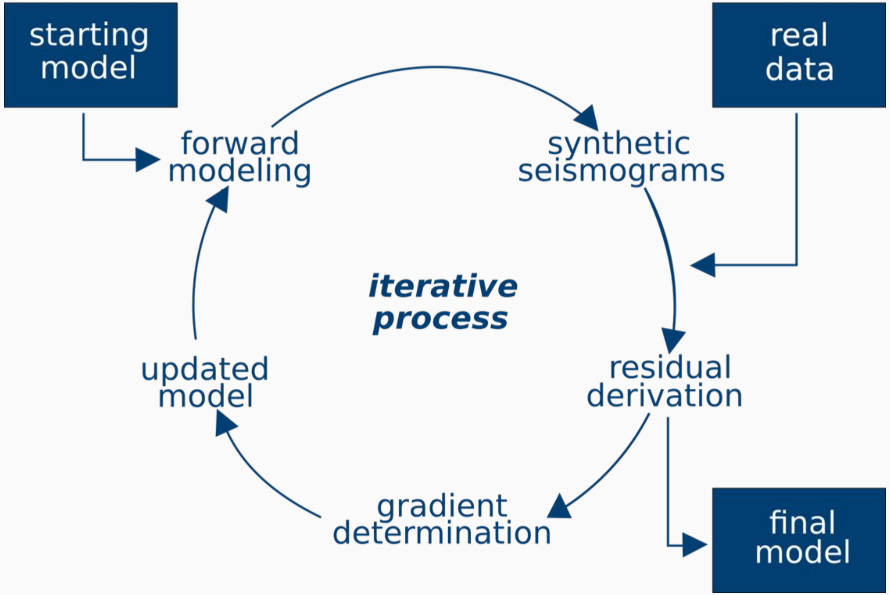

Cartoon by Deborah Wehner

Waveform tomography

To minimise the misfit, its **gradient** is computed. This is done using the **adjoint method** and requires another 3-D wavefield simulation.

The gradient can be seen as a generalisation of the "ray path", but combines the signals of many different events and receivers .

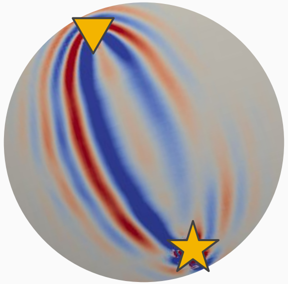

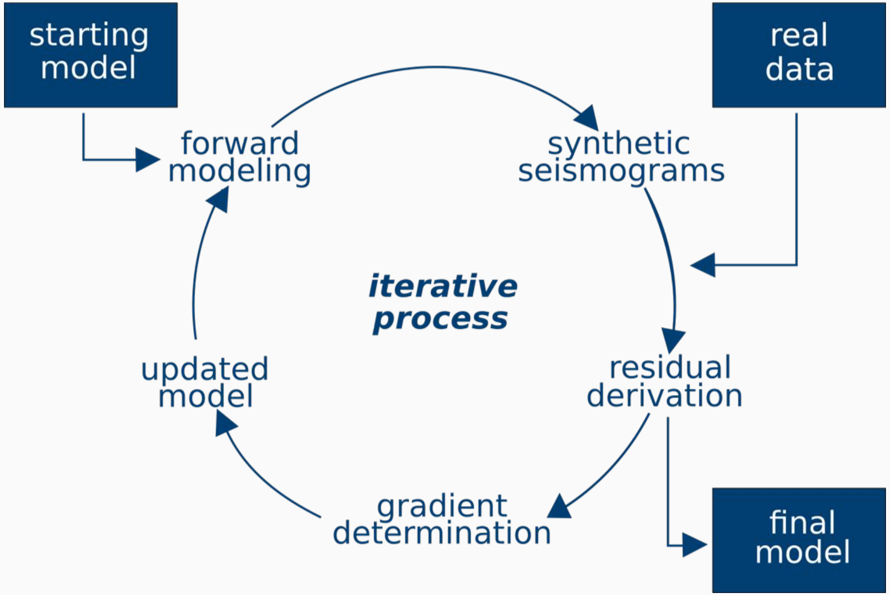

Cartoon by Deborah Wehner

Waveform tomography

Model updates are (usually) made using a gradient-based algorithm (e.g. L-BFGS).

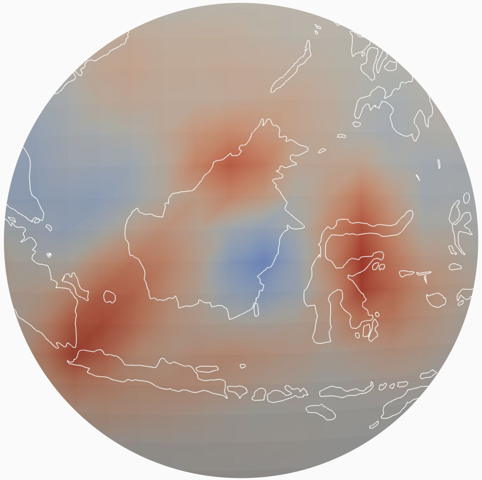

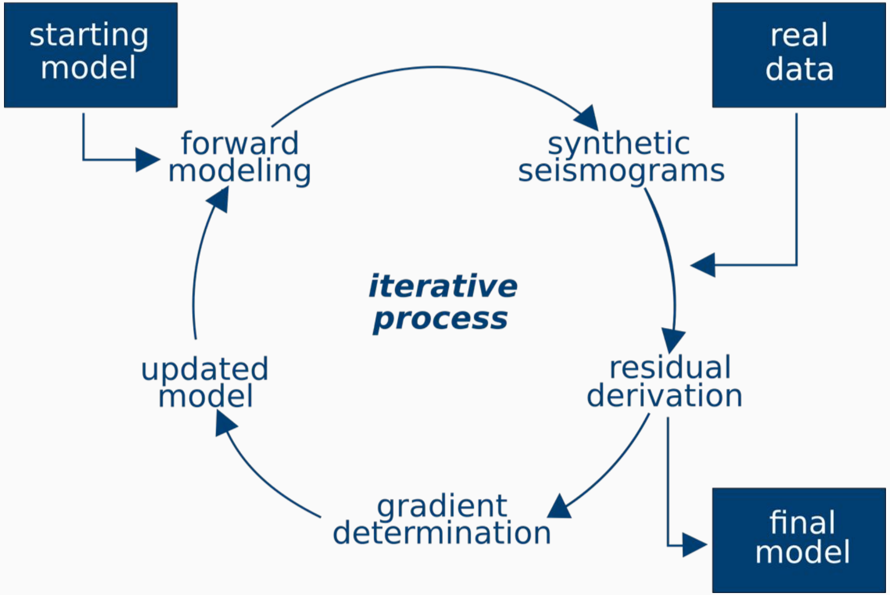

Cartoon by Deborah Wehner

Waveform tomography

So we go from this:

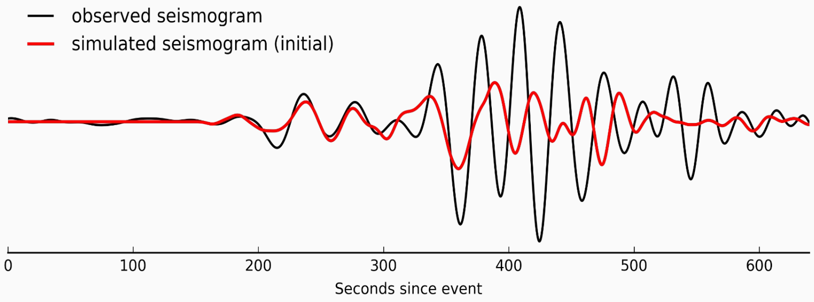

To this:

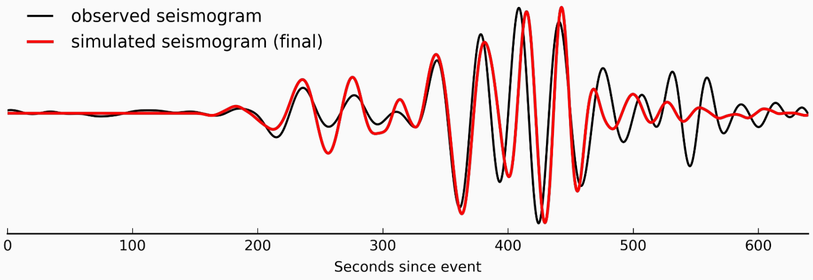

Bonus 2:
Optimising sensitivity to deep structure

Window selection

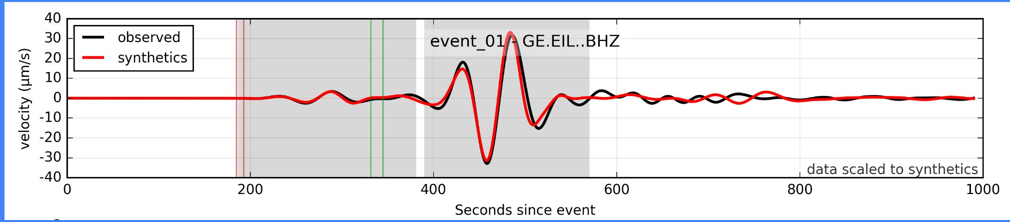

- The selection of windows may be necessary in waveform tomography to avoid cycle skipping or to prevent noise from entering the inversion.
- We optimised our window selection to maximise sensitivity to **deep structure**.
- This is done by **separating small-amplitude body-wave signal** from large-amplitude surface waves.
- Small-amplitude signal is damped in the time-frequency phase misfit *[Fichtner et al, 2008]* as a result of the weighting factor W_p applied to each window (necessary to stabilise the measurement):

$$J_{\mathrm{TF},p}(\boldsymbol{m}) := \int_t \int_\omega W_p^2\left(t,\omega\right)\left[\phi(\boldsymbol{m},t,\omega) - \phi_{\mathrm{obs}}(t,\omega)\right]^2 \mathrm{d}t\mathrm{d}\omega,$$

$$W_p = \frac{\log(1+|\tilde{u}_{\mathrm{obs}}|)}{\max(\log(1+|\tilde{u}_{\mathrm{obs}}|))},$$

- By selecting separate body and surface wave windows, we use the deep body wave sensitivity to maximum effect.

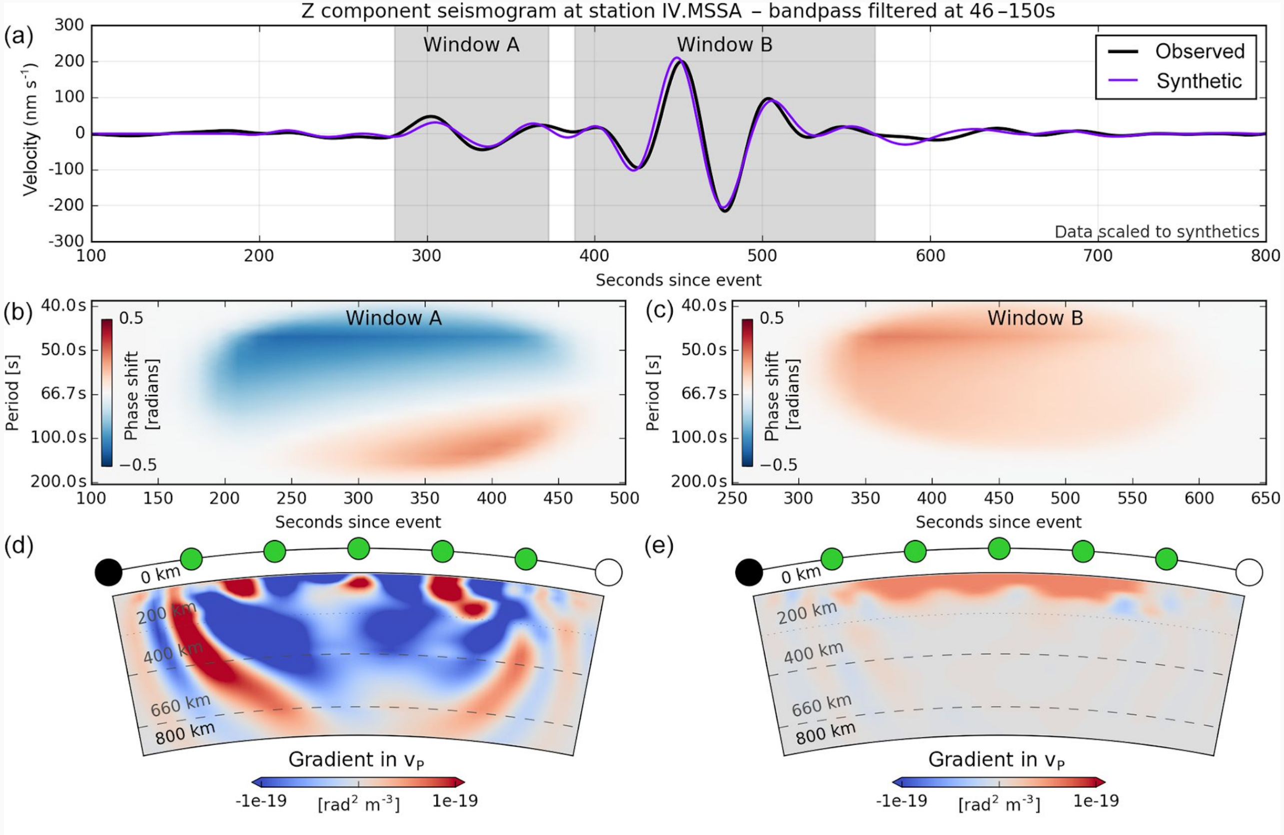

The effect of separate body- and surface wave windows: Because of the misfit functional weighting (W_p), small-amplitude signal is damped even if the signal is robust. This can be solved by picking separate windows for (small-amplitude) body- and (large-amplitude) surface waves, thereby improving depth resolution. **(a)** Observed and synthetic seismograms with two separate windows A and B. **(b)** Weighted time-frequency phase difference $W_p(\phi - \phi_{obs})$ for window A. **(d)** A cross section through the corresponding sensitivity kernel for v_P, showing a deeply dipping body wave. **(c, e)** Phase difference and kernel for window B. Note that both kernels are on the same colour scale. Because B is a surface wave window, it is to be expected that sensitivity to P velocity is much reduced.

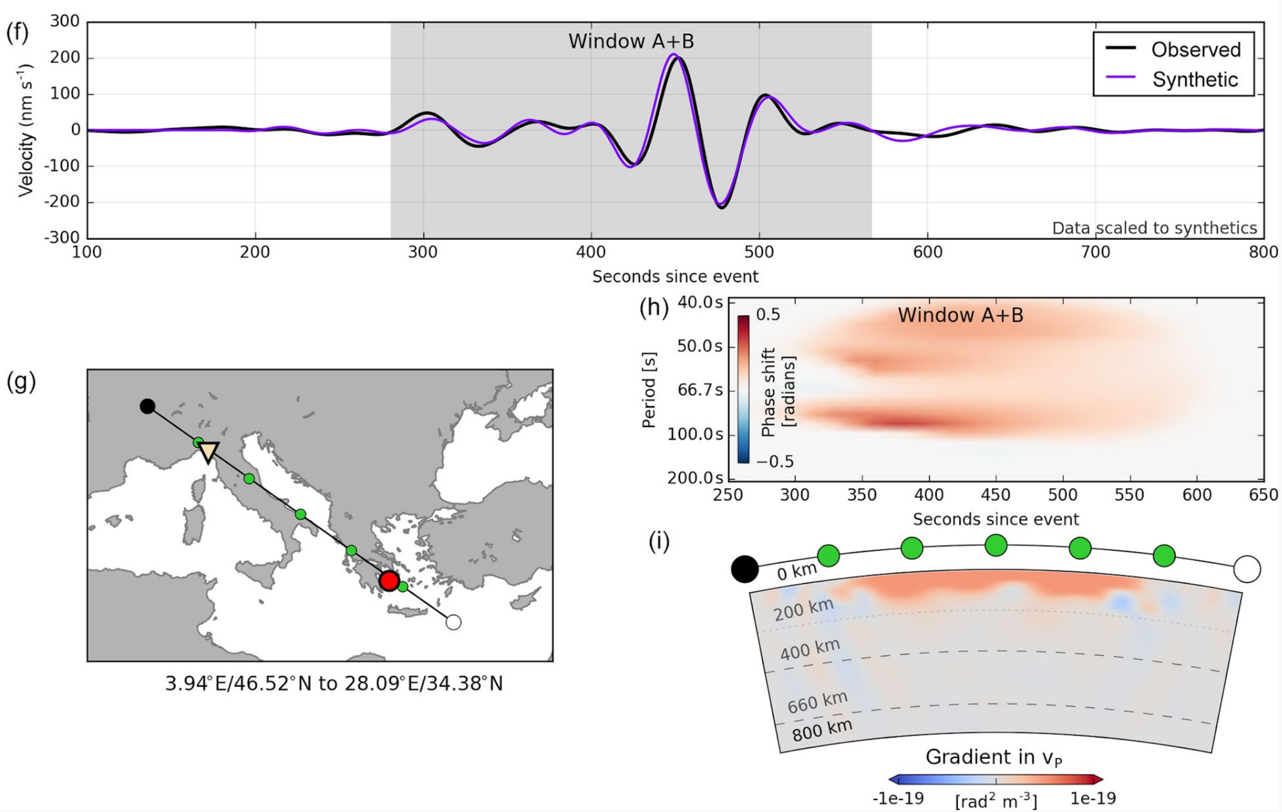

The effect of separate body- and surface wave windows: Here, all data is incorporated in a single window -- possible in principle because the noise level is low and there are no cycle skips. However, because of the misfit functional weighting (W_ϕ), the small-amplitude body-wave signal has hardly any effect on weighted phase misfit and kernel. **(f)** The same traces as in panel (a) but now with a single combined window (A + B). **(g)** Map showing the location of the cross section, with the locations of the earthquake ● and station ▼ . **(h, i)** Phase difference and kernel for the combined window (A + B). Note the similarity to the corresponding plots for window B (c, e) – a result of the weighting W_p that suppresses the effect of the small-amplitude signal.

Bonus 3:
The effect of source errors on tomography

Source information

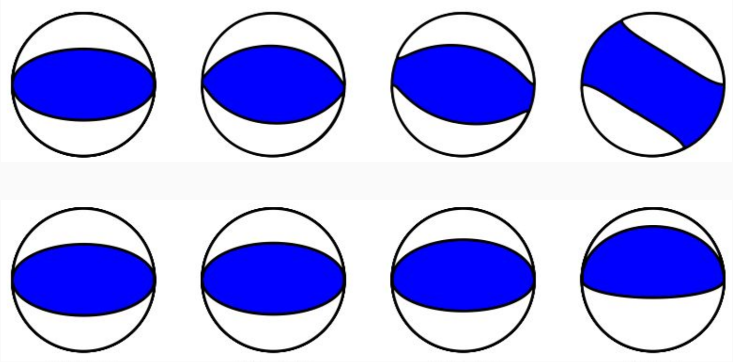

- Usually, source parameters remain constant throughout an inversion.
- However, if (strong) 3-D structure develops, this may not be suitable.
- In general, source parameters are only really "valid" within the framework of data, modelling approach and Earth model in which they were determined.
- This has the potential to affect tomography.

Example 1: shifting a source

- This event showed a slightly suspicious azimuthal pattern of positive and negative phase shifts.
- This could indicate an erroneous location

Figure: see Supplementary Material in [Blom et al, Solid Earth, 2020](#).

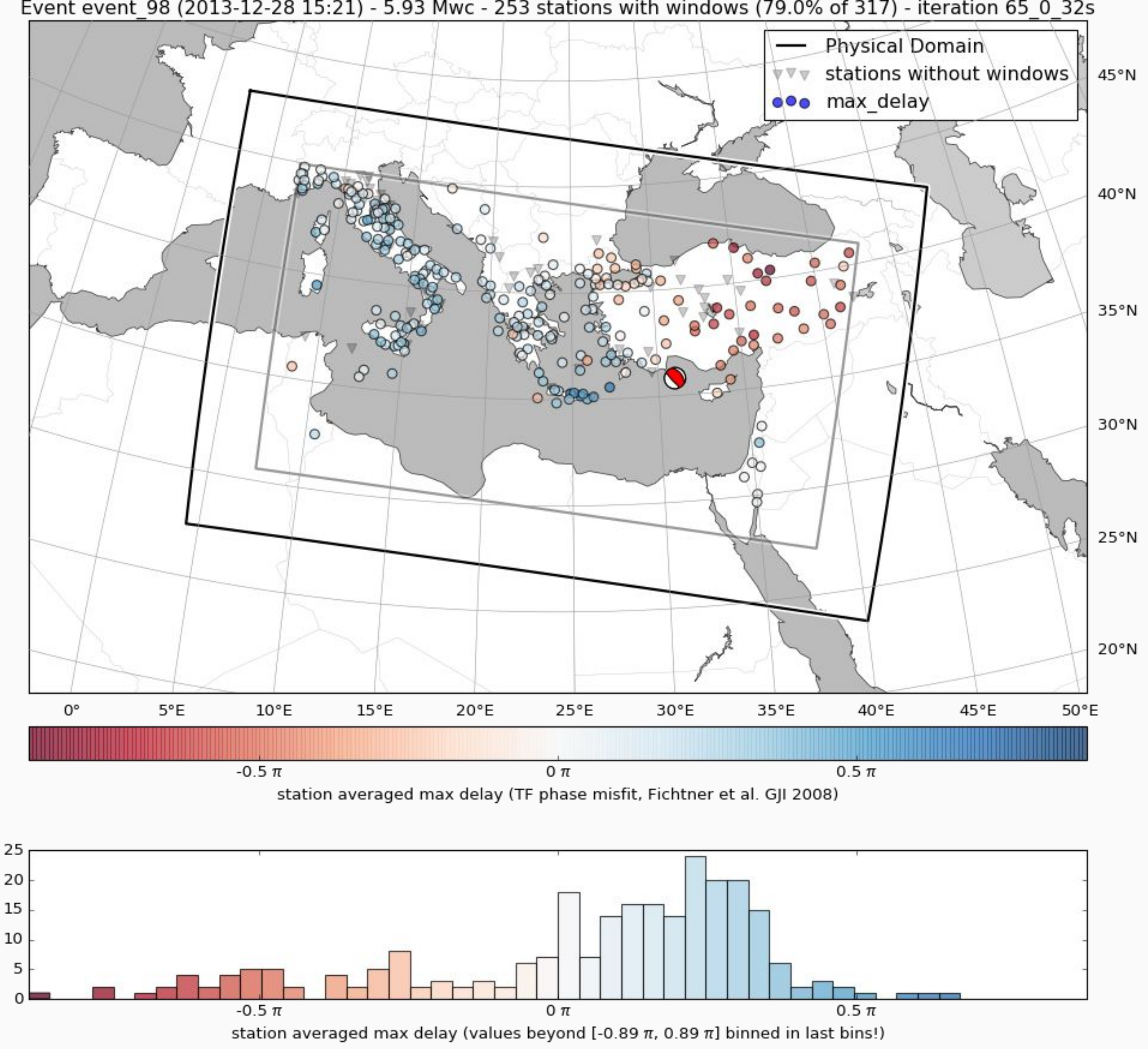

After manually moving the location:

- Shifting the source location slightly to the NE results in a nearly unimodal (and much less strong) pattern of phase shifts.

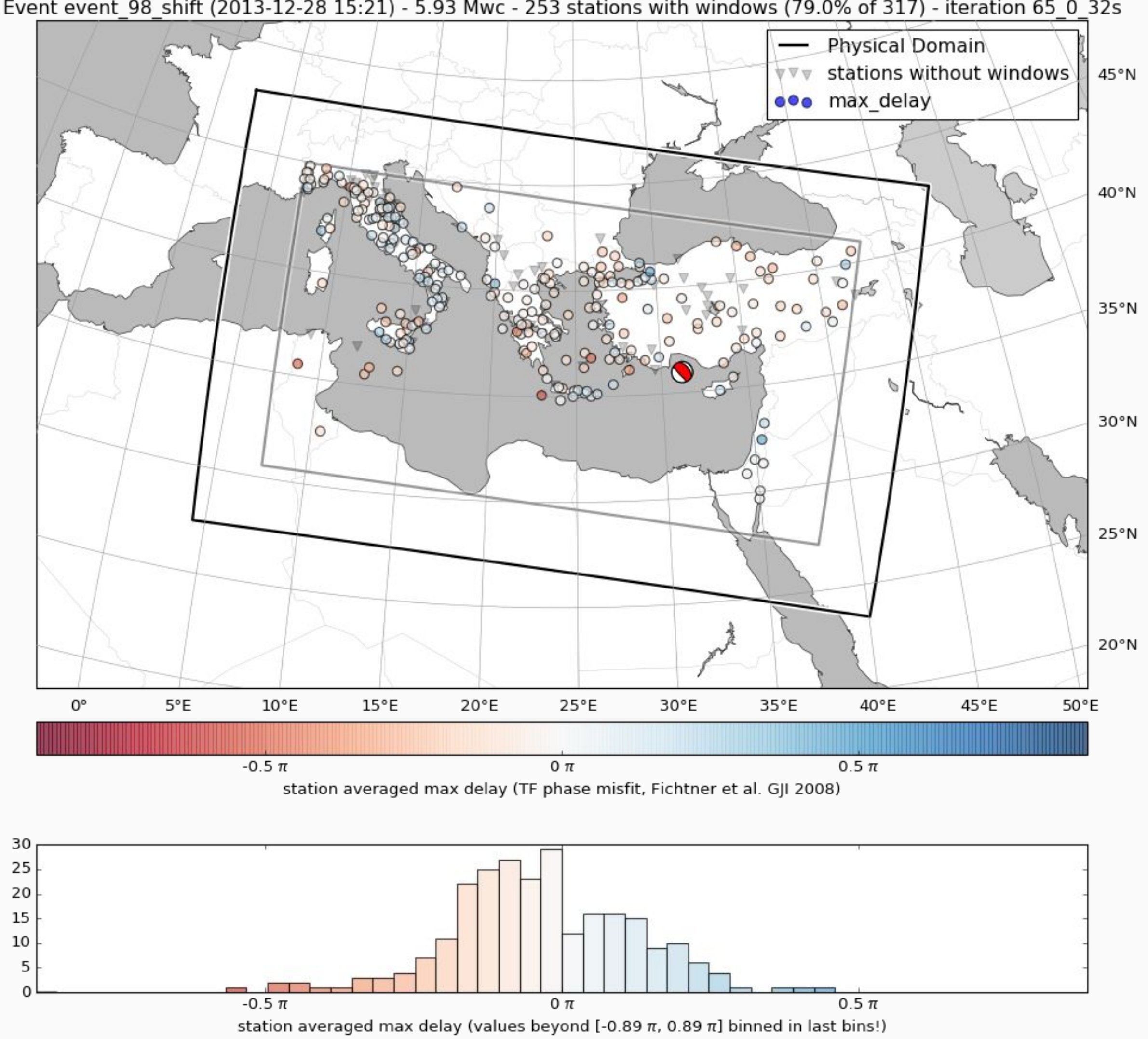

Figure: see Supplementary Material in [Blom et al, Solid Earth, 2020](#).

Example 2: Anomaly E

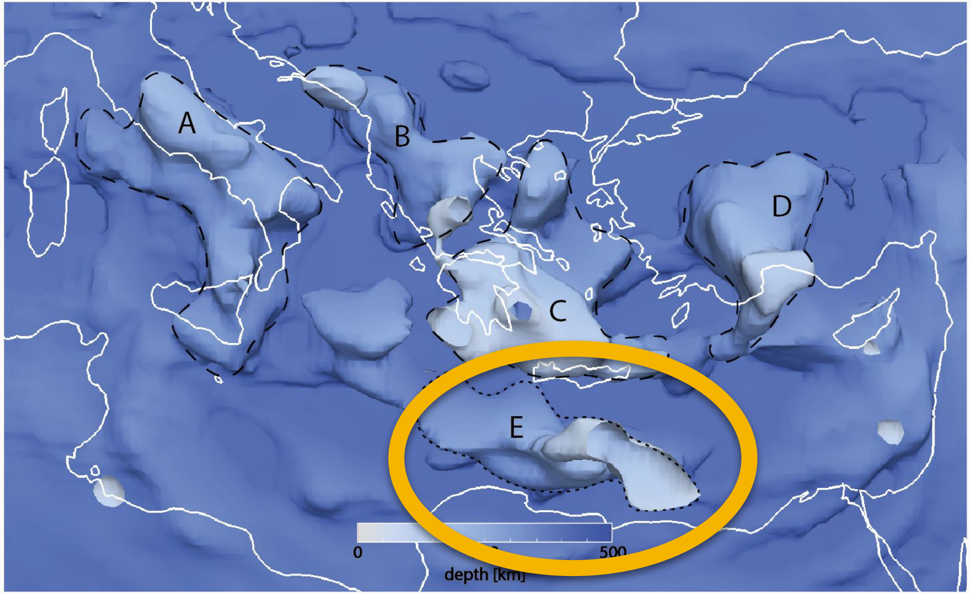

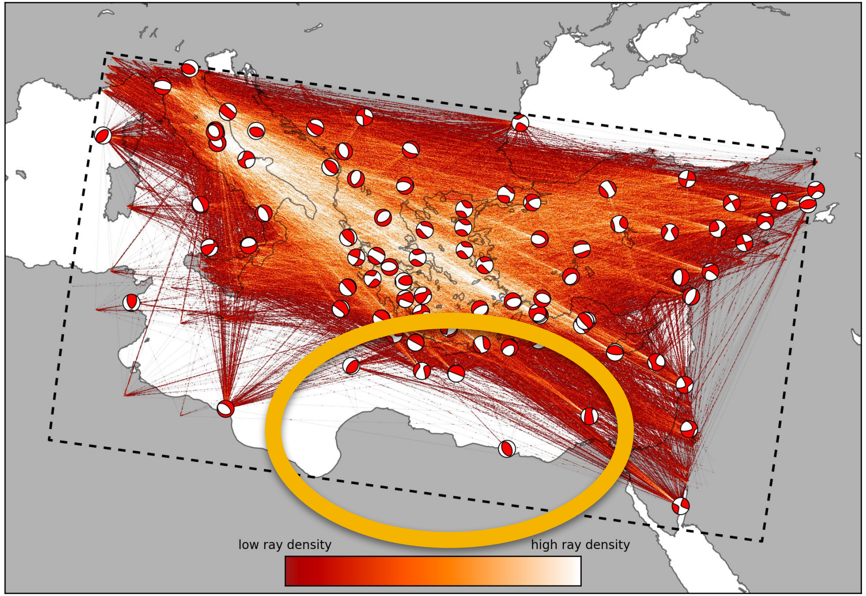

Anomaly E in [Blom et al, Solid Earth, 2020](#) could well be the result of such a source effect. The structure is quite strong, and mostly constrained by a single event in North Africa.

The effect of source errors on tomography

We are currently working on a quantification of the effects of errors in the source parameters on tomography (in particular waveform).

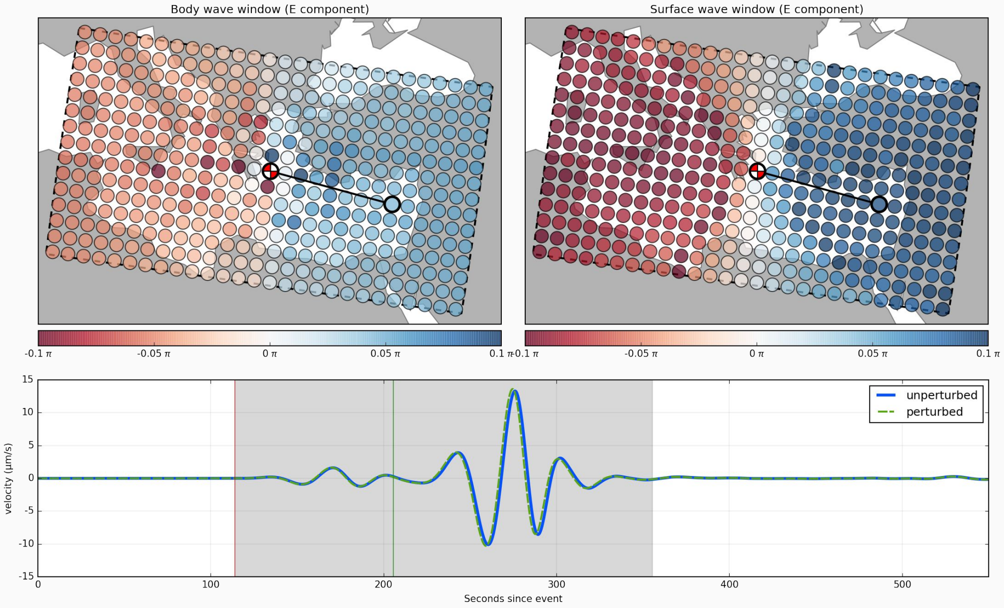

Figure: the effect of a 5 km horizontal shift on measured phase shifts for seismograms filtered between 28--150 s.